R. Stirn, T. Gonzalez Baquet, S.R. Kanjarkar, W. Meier, K.P. Geigle, H.-H. Grotheer, C. Wahl, M. Aigner
Comparison of particle size measurements with laser-induced incandescence, mass spectroscopy and scanning mobility particle sizing in a laminar premixed ethylene/air flame
Combustion Science and Technology 181 (2) 329-349 (2009)

Comparison of particle size measurements with laser-induced incandescence, mass spectroscopy and scanning mobility particle sizing in a laminar premixed ethylene/air flame

R. Stirn, T. Gonzalez Baquet, S. Kanjarkar, W. Meier,

K. P. Geigle, H.-H. Grotheer, C. Wahl, M. Aigner

DLR Institute of Combustion Technology

Pfaffenwaldring 38, 70569 Stuttgart, Germany

Abstract

Particle size distribution functions (PSDF) and mean particle sizes have been determined in a laminar premixed ethylene/air flame with three different experimental approaches. These are photo-ionization mass spectrometry (PIMS) [Grotheer 2004], scanning mobility particle sizing (SMPS) and laser-induced incandescence (LII). The main goal of this investigation was the cross validation of these three methods used at our institute for the determination of particle sizes in a great variety of flames or exhaust gases. We found good agreement between the three methods

in the ranges where they are comparable and furthermore a complementary behaviour for the different size ranges. PIMS and SMPS are able to measure the particle size distribution functions with good resolution. PIMS is favorable in detecting the smallest particles ($< 6\ nm$) and thereby able to detect even bimodal distributions of the soot precursor particles. SMPS and LII are suitable in the mid and upper range of the particle sizes ($> 2\ nm$ and $> 3\ nm$, respectively). LII offers the particular advantage of beeing a non-intrusive method. This makes it applicable in extreme environments, like high pressure flames, as well as in very sensitive flames because no probe is needed.

1 Introduction

In the last years public awareness for emission of particulate matter into our environment has grown rapidly, and great efforts are being undertaken to reduce its emission. However, the formation of soot in technical flames or engines is still not completely understood. Therefore it is necessary to gather information about soot precursors and the young soot particles in flames as detailed as possible. For this purpose we investigated well defined premixed ethylene/air flames with three different methods: photo ionization mass spectrometry (PIMS), time resolved laser-induced incandescence (LII) and scanning mobility particle sizing (SMPS). Particle properties as size distributions are important to validate kinetic soot models [Braun-Unkhoff 1998], [Zhao 2003] which are essential for the understanding of soot formation and hence for further improvement of combus-

tion devices. In agreement with other publications [Grotheer 2004], [Zhao 2005], [Singh 2005], [Maricq 2006] we found bimodal distributions at different flame conditions. These bimodal structures can originate from different processes, because of different fuels and flame conditions used. One possible explanation for the bimodality of particle size distribution functions is the competition between nucleation of soot precursors and the subsequent coagulation of these precursors to soot. A detailed description of this model can be found in [Zhao 2003], as well as references for other possible explanations of the bimodal structures.

In this contribution we compare the different experimental methods and discuss their complementarity, including advantages and limitations. As a non-intrusive method with high spatial resolution, LII has rapidly become the favorite method for soot volume fraction measurements in various combustion processes [Santoro 2002]. Because the decay rate of the LII signal depends, at least at low laser fluences, on the surface area of the particle, this characteristic can be used to measure the particle size [Michelsen 2007]. However, it is not possible to determine particle size distributions or to identify bimodal size distribution, because the contribution of small particles to the emitted radiation is very small. The method has the advantage that no probe is needed and that it can be applied without interacting with the flame. Additionally the effort needed to apply LII in pressurized flames is smaller than applying a probing method, because no lead-through for the sampling line or cooling of the probe is needed. Even flames with high soot concentrations can be studied since probe clogging is not an issue for LII. The most obvious advantage of the other meth-

ods is their ability to resolve the particle size distribution functions. PIMS is a well-established technique for the sensitive detection of atoms and molecules and it has been further developed in our institute for the measurement of small particles [Grotheer 2004]. It is able to measure even the smallest particles, but it has its upper detection limit at particle diameters of about 6 nm. SMPS is very useful in the mid and upper range of particle sizes (> 2 nm). In the investigations presented here, a commercial system was used and great effort has been made for the extraction of the particle laden gas probe from the flame.

One goal of this study was the comparison of the results obtained with the different measurement techniques and to assess their potential for further investigations in sooting flames. A further goal was the extension of the data base from the flame investigated which already has become a "standard flame" within the International LII Workshop [Schulz 2006]. Although this study attempts to provide quantitative data concerning size distributions no attempt is made at present with regard to the determination of particle concentrations.

2 Experimental and Results

2.1 Burner and flame parameters

The investigated ethylene/air flames were stabilized on a stainless steel water-cooled porous plug burner (McKenna) with a fixed total gas flow of 10 sl/min and an uncertainty of the flow-controller calibration in the range of 1-2 %. The burner consists of an porous plug with a diameter of 60 mm and an annular

porous plug with an inner diameter of 61 mm and an outer diameter of 73 mm. To prevent flame flickering the flame was stabilized by a cylindrical steel plate with a thickness of 20 mm and a diameter of 60 mm, fixed at a height above the burner (HAB) of 21 mm. Alternatively the flame has been stabilized by means of a nitrogen shroudflow, to allow measurements at higher HAB. Two main parameter variations have been performed. First the equivalence ratio Φ of the flame has been changed from 1.8 to 2.6 with the measuring position fixed at 12 mm above the burner surface. Second, the measurement position has been changed from 8 mm to 16 mm above the burner surface with a fixed equivalence ratio of $\phi = 2.1$. These variations were carried out for all three diagnostic methods. Additionally, the flame behaviour was studied in more detail by qualitative LII. To be sure that there are no errors due to insufficient thermalisation we measured the incandescence signal at 1, 7, 12 and 18 minutes after ignition of the flame. We found no significant change in the LII signal decay, and hence in local flame temperature and particle properties after 7 minutes. Therefore all measurements have been started 7 minutes after ignition of the flame at the earliest, so that a stable flame was ensured.

Moreover the different stabilization methods, stabilization plate and nitrogen shroudflow, have been investigated by comparing the incandescence signals. Like Axelsson [Axelsson 2000] we found no influence of the stabilization plate on the decay curves at the standard measuring height of 12 mm above the burner surface. Neither placing the plate 21 mm or 31 mm above the burner, nor omitting it and replacing the stabilization plate by a 70 sl/min nitrogen shroudflow

changed the LII signal decay.

2.2 Laser-induced incandescence

Laser-induced incandescence is a non-intrusive method which can provide informations about soot concentrations and soot particle sizes, the latter if the time resolved incandescence signal is recorded. For the determination of particle sizes one has to simulate the incandesence signal by a numerical model and compare it with the measured one. In the last few years there have been many advances in modelling LII considering heating by absorption of laser energy, cooling by heat conduction to the surroundings, sublimation and radiation [Melton 1984]. Other processes like annealing, oxidation and photodesorption have been included in the models recently [Michelsen 2003], [Schulz 2006]. For this work the model of Michelsen has been implemented in Matlab/Simulink. This implementation accounts for absorption, conduction, sublimation, radiation, annealing and oxidation, only photodesorption has been neglected. In deviation from the model of Michelsen [Michelsen 2003] some input parameters for the model, namely the refractive index function (0.42 at 1064 nm) and the thermal accomodation coefficient (0.37 instead of 0.3) are experimental values taken from another source [Snelling 2004].

In our experiment we detected the incandescence signal, resulting from soot particles heated with a Nd:YAG laser pulse up to about 4000 K, with fast photomultipliers at two different wavelengths, each with an aperture of 0.8 times 2 mm. The laser pulse was emitted at a wavelength of 1064 nm and had a

FWHM of about 7 ns. The lasersheet was formed by a cylindrical negative lense with a focal length of $f = -80\ mm$ and a spherical positive lens with a focal length of $f = 1000\ mm$. The resulting lasersheet had a thickness of 0.4 mm and a height of 8 mm at the measuring position. The detection wavelengths were at about 400 nm ($\Delta\lambda \approx 15\ nm$) and 700 nm ($\Delta\lambda \approx 40\ nm$). The detection of the signals is perpendicular to the incident laser beam. The measurement of the LII signals at two different wavelengths allows for the determination of the particle temperature [Kock 2006]. This provides an independent way to determine the particle temperature, and hence, validate the results of the LII model. In Fig. 1 the experimental setup for the LII measurements is shown.

Due to a potential change of the original particle size when evaporating and due to the lack of understanding of the evaporation process it is helpful to reduce evaporation as far as possible. Therefore the measurements have been performed with fluences of 0.18 J/cm^2 to 0.25 J/cm^2 because in this case evaporation is minimized. The use of even lower fluences would lead to a significantly worse signal to noise ratio.

In Fig. 2 the LII decay curves for different equivalence ratios between $\Phi = 2.0$ and $\Phi = 2.6$ and the resulting particle diameters are shown assuming monodisperse particle sizes for the data evaluation. The incident laser energy density was constant at about 0.21 J/cm^2 where no significant evaporation peak is observed. Hence, in this and the following figures the signals are normalized to their maximum value. With increasing equivalence ratio the decay time also increases. This is due to an accelerated growth of the soot particles because of

the higher amount of soot precursors in a richer flame.

The following two figures display the temporal behaviour of the incandescence signal and the resulting particle diameters for different positions above the burner surface for the equivalence ratios $\Phi = 2.1$ (Fig. 3) and $\Phi = 2.3$ (Fig. 4). The decay times are increasing with increasing HAB, i.e. reaction time, due to the growth of the soot particles. Moreover changing equivalence ratios and heights above the burner lead to a change of flame temperatures and aggregation processes influencing the decay time of the incandescence signal [Axelsson 2000]. In this case the apparent decrease of the particle sizes at 15 mm above the burner is mainly due to the fact that the flame temperature is assumed to be constant at 1700 K for all heights above the burner, while in reality the temperature decreases as soon as soot is formed and radiates [Tsurikov 2005]. The deviation of the assumed gas temperature never exceeds 100 K up to a height of 14 mm above the burner [Malarski 2005]. For equivalence ratios from 2.1 [Malarski 2005] to 2.7 [Brackmann 2002] the gas temperatures are also in the range of $1600 - 1800$ K. For the standard measuring point at an equivalence ratio of 2.1 and a HAB of 12 mm a change of the gas temperature of 100 K resulted in a deviation of 1 nm.

Considering the uncertainties of the high number of input parameters for the model, the error due to assumption of monodisperse particle sizes [Bladh 2004] and the uncertainties due to the measurement of the laser beam properties, like fluence and sheet width, we estimated an error for the particle sizes of about 30%.

2.3 Photo-ionization mass spectrometry

For the measurements presented below a high resolution time-of-flight mass spectrometer (Stefan Kaesdorf GmbH) was used. This device provided an unusual large measuring range up to several hundred thousand atomic units (u) and a high sensitivity due to high voltage ion optics, a high acceptance volume and the corresponding high sensitivity detector.

In addition, the sampling system was especially designed to expand the sample from atmospheric pressure to the high vacuum chamber of the MS. For the sampling of flames and other practical systems (e.g. engine exhaust pipes) at atmospheric conditions a differential pumping system was used. As sketched in Fig. 5 the sample was continuously drawn through the nozzle (0.8 mm in diameter) of a quarz glass probe (i.d. 6 mm). Downstream a small portion of this flow was extracted from the main flow by means of a solenoid valve forming a pulsed T-piece. The pulsed flow expanded through a nozzle-skimmer system to form a molecular beam which was subsequently ionized. As shown in Fig. 5 our earlier so-called cross-beam arrangement as used in previous studies [Gonzalez Baquet 2005],[Thierley 2007] was replaced by an axial arrangement. Cross-beam ion sources were recommended for the earlier linear time-of-flight instruments because the neutral beam can lead to a contamination of the multiplier. By using a reflectron time-of-flight mass spectrometer this risk is largely overcome. The advantage of the axial geometry is that ions and the neutral beam travel in the same direction. Problems of inertia to which heavy ions are particularly sensitive, are thus avoided. The result is that axial-beam

spectra generally extend to higher masses.

The pressure drop due to expansion of the sample in the nozzle and its resulting cooling quenched possible reactions. In addition, this expansion reduced the extent of coagulation in the sampling line, a common problem when measuring soot precursor particles in flames by means of intrusive methods [Maricq 2004]. Complementary measurements [Gonzalez Baquet 2008] demonstrated that the extent of coagulation and other sampling line effects, like surface growth or particle wall losses, are small enough to assure a good characterization of soot precursor particles in flames by means of time of flight mass spectrometry. The residence time of the sample in the sampling line was calculated to be approximately 10 ms.

The photo ionization of the sample was provided by an ArF excimer laser (Lambda Physik OpTex) at $\lambda = 193\ nm$. The laser produced pulses with a FWHM of 10 ns at repetition rates of up to 200 Hz. Special care was taken on the proper ionization of the particles in study. Complementary measurements [Gonzalez Baquet 2007] showed that these particles are characterized by a very low fragmentation threshold. Consequently, low laser power densities around 0.12 MW/cm^2 were routinely used. This is another important improvement relative to our earlier study [Thierley 2007]. Measurements at different equivalence ratios (Φ) and heights above the burner (HAB) were carried out. First, for a fixed $HAB = 12\ mm$ a series of measurements was conducted at different equivalence ratios ranging from $\Phi = 1.76$ up to 2.28. Some of the results are shown in Fig. 6. For each of the operation conditions several repe-

titions were carried out. The general features of the distributions (number of modes, maxima, widths of the distribution curves) were well reproducible, however, the intensity of the ion signals showed strong fluctuations, in some cases, up to a factor of 6. Each of the particle mass distributions presented in Fig. 6 are averages of all measurements at the same conditions. As shown in Fig. 6, the measured particle mass distributions are not unimodal, rather up to three different modes (A, B, C) have been observed. Mode C is considered to consist of primary soot particles. Mode A and mode B, on the other hand, represent soot precursor particles, see discussion.

Soot precursor particles (mode A and mode B) emerge in the flame at equivalence ratios slightly below the sooting threshold ($\Phi = 1.80$). These particles show increasing number concentrations and increasing particle masses for richer flames. The particles constituting mode A are observable along the whole investigated stoichiometry range while particles constituting mode B are just observable for $1.76 < \Phi < 1.89$. Above this limit mode B is probably not distinguishable due to an excess of mode A.

Mode A is obviously found under slightly leaner conditions than mode B. For both modes a strong dependence of concentrations and mass distributions on Φ is found. The observed drop of concentration when approaching the sooting threshold from the rich side has already been reported in our earlier study [Thierley 2007].

For soot particles (mode C) an unexpected behavior is observed. Soot particles, as described in the literature, are characterized by an increase in particle

size, and consequently in particle mass for an increasing equivalence ratio. This behavior is not observed in the present measurements as mode C becomes detectable at $\Phi \geq 1.85$ without any significant change of the maximum mass of approximately 200000 u upon increase of Φ (see inserts in Fig. 6). Although ions of higher masses are detected our instrument is obviously not capable of correctly resolving mass distribution curves in this size range.

In addition, for $\Phi = 1.8$ and $\Phi = 2.1$ mass distribution curves were measured as a function of HAB. To this end, the position of the probe above the burner was varied in 2 mm-steps. Due to geometric constraints the range extends from 6 to 16 mm above the burner surface. Some typical results are shown in Fig. 7 and Fig. 8.

In general, for increasing heights above the burner, an increase of the signal intensities along with a slight shift towards larger masses is found for soot precursor particles. The persistence of soot precursor particles along the flame axis suggests their permanent de novo formation from the gas phase as otherwise losses by coagulation or oxidation would reduce their signal intensities.

Once again, soot particles (mode C) do not show the expected behavior known from the literatur since these particles are supposed to grow in size along the flame due to surface growth and coagulation. In the measurements presented above, however, no significant shift of mode C towards larger masses is distinguishable.

Mass distribution curves were transformed into size distribution curves by assuming spherical particles. For this transformation, information about the

density of the particles is necessary. According to Dobbins [Dobbins 2002], soot precursor particles have a density close to 1.2 g/cm^3, while carbonaceous soot particles are characterized by a density of 1.8 g/cm^3. Thus, two different values were used for the calculations: For the low mass range ($< 100000\ u$), where the ion signals are interpreted as soot precursor particles, $\rho = 1.2\ g/cm^3$ is used. Above 100000 u $\rho = 1.8\ g/cm^3$ is considered more adequate. From the size distributions so obtained, the sizes at maximum signal intensity were taken and plotted as "mean particle diameters" in Fig. 9. In the case of mode C, the resulting diameters are only plotted for $\Phi > 2.00$ because at lower Φ values the soot signals were too weak to extract any reliable information.

In the same way, information about the evolution of the particle diameter along the axis of the flame was obtained from the measurements at variable HAB.

When using time-of-flight mass spectrometry, the time that ions require from their ionization to their detection is recorded. To this end, the signals coming from the detector during a specified time interval or bin are recorded and summed up. In our case, these bins are characterized by a constant width that defines the resolution of the measurements. Using a mass calibration routine, this information is subsequently transformed into ion mass data. Unfortunately, since the time of flight is proportional to the square root of the mass-to-charge ratio of each ion, an error is introduced when transforming the time of flight into ion mass values using a constant bin width. This error is negligible in the case of light ions but gains in importance when measuring heavy ions.

In the latter case a fairly large bin width (e.g. 1024 ns) must be used. Consequently, a bin comprises several ion masses. The signal intensity per bin results from the addition of all the counts corresponding to all ion masses comprised in the bin. Due to the relation between time of flight and ion mass, for increasing time of flight the number of ion masses per bin increases. For this reason, given a constant number of counts per ion mass, the apparent signal intensity per bin will increase with increasing time of flight. Since particle mass distributions result from the envelope of the detected mass spectra, this effect leads to a shift of the mean particle mass towards larger masses.

The extent of this effect depends on the shape of the mass distribution and leads to an overestimation of the mean particle mass. In our case, the resulting error is estimated to be $\leq 30\%$ in terms of mass. Considering $d \propto \sqrt{m}$, this relative error of $\leq 30\%$ is reduced to just $\leq 10\%$ in terms of particle diameter. This error is considered small enough to allow the quantitative comparison with other measuring techniques like SMPS, TEM or LII.

2.4 Scanning Mobility Particle Sizing

Scanning mobility particle sizing for the measurement of soot particle size distributions in laboratory flames has gained a lot of attention in the recent past [Kasper 1997], [Zhao 2003a], [Maricq 2004]. This technique provides the opportunity of following the soot particle dynamics in flames with the ability to measure particles as small as 2 nm. Reliable probe sampling, which minimizes the effects of particle coagulation and diffusion wall losses, is an important factor

that has to be taken into consideration using this type of particle measurement technique. The experimental setup with an emphasis on the description of the sampling probe is presented in the following section.

The experimental setup is schematically shown in Fig. 10. The sample probe is a stainless steel tube of 6 mm outer diameter with a wall thickness of 1 mm. This tube has a concentric inner tube of 3 mm outer diameter and a wall thickness of 0.7 mm. The outer tube has an orifice with a diameter of 0.5 mm. The sampling probe is positioned along the central line of the burner matrix with the orifice facing towards the burner surface. The position of the inner tube was fixed so that the distance between the end of the 3 mm tube and the orifice is 12 mm. The high nitrogen flow (50 l/min) from the 3 mm tube creates a low pressure region near the orifice. This causes the suction of the flame gases inside and immediate dilution and cooling [Zhao 2003a]. There is an opportunity of further dilution by splitting the flow into two streams and adding fresh diluting gas. Two such additional dilution units were used in the experiments, see Fig. 10. The dilution ratios were determined by measuring the CO_2 amount from a stoichiometric flame with FTIR. The measured dilution ratios were well above 10000 times which is good enough to preserve the original particle size distributions, as in the flame, by the time they are measured by SMPS. The residence time of the sampled particles from the sampling orifice to the inlet of the instrument was less than 300 ms.

The effect of the sampling probe on the flame temperature is reported in the literature [Zhao 2003a]. It was reported that the probe reduces the local flame

temperatures. But when the sample probe was placed at a distance sufficiently remote from the intense flame zone, the probe has a minimal effect on the maximum flame temperature.

A TSI SMPS Model 3080 was used in the present study. It consists of a Kr-85 bipolar charger, nano differential mobility analyzer model 3085 for particle sizing and an ultrafine condensation particle counter (UCPC) model 3776. The experiments were performed under high flow conditions ($1.5\,l/min$). The typical SMPS settings of 120 s up scan and 15 s down scan were applied to collect the particle size spectra. Sampled soot particles were transported from the sampling probe to the inlet of the SMPS using silicone conductive tubing with an inner diameter of 5.1 mm and a length of 600 mm.

As mentioned in the previous sections, experiments were conducted at different equivalence ratios ($1.8 - 2.2$) and at different heights above the burner matrix HAB ($6 - 14\ mm$). Experiments were performed by applying different dilution rates until the point where there was no further effect of dilution on the collected particle size distributions. At lower heights in leaner flames, where the particle number concentration is less, low dilution rates (≈ 4000) were sufficient. Higher dilution rates (≈ 10000) were needed at higher HAB and higher equivalence ratios. At lower equivalence ratios the sampling probe showed good reproducibility for a time of 15-20 minutes, but at an equivalence ratio higher than two, the orifice of the probe had to be cleaned after every 4 measurements. For each operating condition, 3-4 spectra were collected which showed good reproducibility in both mean diameter (with max. error limit $\pm$ 10%) and number

concentrations (with max. error limit ± 15%).

Particle size spectra collected in experiments performed at 12 mm HAB and different equivalence ratios are presented in Fig. 11. Since different dilution rates were used at different measurement points, the particle size distribution functions normalized with respective number densities measured by SMPS are reported.

Bimodal distributions, interpreted as consisting of a soot precursor mode and a soot mode, were observed starting from an equivalence ratio of 2.0. This type of bimodality is reported to be dependent on flame temperature and it occurs because of the existing competition between particle nucleation into the mass growth region and particle-particle coagulation [Zhao 2005]. In our experiments, both modes of particle size distributions were observed to be log-normal, unlike to the reported combination of power-law (smaller mode) function and a log-normal (bigger mode) [Zhao 2003a]. The reason for this could be the extended lower measurement limit (2 nm) of the instrument used in our experiments, which gives the opportunity to study the particles of size below 3 nm. For the particle size range below 3 nm the counting efficiency [TSI] shown in Fig. 12 was considered. While the mean diameter of the first mode was only slightly increasing, the mean diameter of the second mode was observed to be increasing with increasing equivalence ratio.

The transition in the particle size distributions from monomodal to bimodal was observed to occur for different equivalence ratios at different heights above the burner. While the transition was observed for $\Phi = 1.9$ at $HAB = 14$ mm,

it was already observed at $HAB = 8\ mm$ for $\Phi = 2.1$.

Fig. 13 depicts the particle size spectra collected at an equivalence ratio of 2.1 and at different HAB. The first bimodal distribution was observed at experiments with HAB of 8 mm. The mean diameters of both - the first and the second mode were observed to be generally increasing with increasing HAB. The smaller mode which corresponds to the soot precursor particles appears to be more dominant with increase in the HAB till 12 mm and remains unchanged upon further increase in HAB.

The main trends of changes in the particle diameters of particle size spectra measured at 12 mm height and at different equivalence ratios are presented in Fig. 14.

3 Summary and Discussion

Three different particle sizing methods have been applied to a well defined premixed laminar ethylene/air flame burning on a watercooled, sintered stainless steel porous plug burner. The flame was investigated at different equivalence ratios, ranging from 1.8 to 2.6 and at different heights above the burner surface, ranging from 6 mm to 16 mm. Different flame stabilization methods have been compared to be sure that there is no significant influence on the flame at the measuring points. By measuring an incandescence signal for every stabilization method at the same point it has been verified that the signals are nearly identical. For the measurements we stabilized the flame with a steel plate which

was fixed at a height of 21 *mm* above the burner surface. Additionally we investigated the thermalization behavior of the flame, again by measuring the incandescence signal, and found that the flames become stable within less than seven minutes after ignition. The main goal of this work was the comparison of the three different particle sizing methods: Scanning mobility particle sizing, photo ionization mass spectroscopy and time resolved laser-induced incandescence. In the following the results of these measurements with respect to particle size and the advantages and disadvantages of each method will be summarized and discussed.

Scanning mobility particle sizing is suitable in the mid and upper particle size range and it is, as well as photo ionization mass spectrometry, able to measure the particle size distribution functions. This ability is indispensable for the detailed understanding of soot growth in flames. In the previous literature [Grotheer 2004], [Zhao 2005], [Singh 2005], [Maricq 2006], as well as in our own measurements, several flame conditions with bimodal structures have been found. The mechanisms responsible for mono- or bimodal structures in the particle size distribution functions have not yet been identified. Therefore it is nessecary to gather as much detailed information about the psdf's in flames as possible. The main challenge with SMPS is the probing method, as an appropriate way of collecting and diluting the sample is essential for the quality of the measurements. In section 2.4 the sampling method chosen for SMPS in this work is described in detail and, in the corresponding Fig. 10, a sketch of the probing setup is shown. Besides the requirement to prevent coagulation and

agglomeration in the sampling line there is the general problem of clogging of the sampling orifice in strongly sooting flames. That is the main reason why the SMPS and PIMS measurements are limited here to flames with equivalence ratios up to 2.3. SMPS is in principle able to measure larger particles than those presented in this work, whereas the PIMS setup has an intrinsic upper limitation at about $6 - 10\ nm$. The general setup for the PIMS measurements and the probing method is described in section 2.3 with a sketch in Fig. 5. In comparison to our earlier MS study [Thierley 2007] two major improvements were achieved, (i) use of an axial beam inlet and (ii) use of much lower photon densities. While the axial inlet improves transmission for heavier ions, the low densities avoid fragmentation which otherwise would shift a mass distribution function to lower masses. Consequently both changes should yield mass profiles with an enhancement at higher masses. Whether these "new" profiles are "true" remains unclear and this was one of the reasons for the cross validation presented in this paper. Definitely we have indications that we suffer a sensitivity drop for masses in excess of several 100.000 u. Nevertheless two statements are possible at present:

- By using extremely low photon densities around 100 kW/cm^2, i.e. 30 times below the value common for gas phase species it was possible for the first time to measure mode A particles by PIMS wich become fragmented at higher fluences [Gonzalez Baquet 2007].

- As indicated by Fig. 6 these ions suffer an intensity drop in the vicinity of the sooting threshold as reported in our earlier study [Thierley 2007]. The sooting

threshold of our present setup is apparently somewhat lower.

The main advantage of PIMS is the fact that no lower instrumental threshold for the particle size detection exists, even the smallest particles can be detected. Additionally, PIMS is able to resolve finer structures in the particle size distribution function. The apparently monomodal soot precursors detected with SMPS turned out to consist of two different modes itself when measured with PIMS. This feature is new and is discussed in more detail in companion publications [Gonzalez Baquet 2007], [Gonzalez Baquet 2008]. Very recently, bimodality of soot precursors has been found using DMA by other groups, too [Sgro 2007], [De Filippo 2007], [De Filippo 2007a]. The capability of detecting several modes is one of the big advantages of PIMS and SMPS. For LII, however, the distinction of lower modes is not possible. With laser-induced incandescence, see setup in section 2.2, it is not possible to get direct information about the shape of the particle size distribution function because of the fact that the emitted incandescence signal is proportional to the square of the particle diameter. Therefore, the signals of significantly smaller particles can not be distinguished in the presence of larger ones. One of the main advantages of the non-intrusive laser-based method is that no sampling is necessary and hence no problems of coagulation nor any disturbances of the flame occur. The LII measurements have been conducted up to an equivalence ratio of 2.6 and even richer flames can be investigated when necessary. No upper particle size detection limit is given a priori and the method can easily be applied to pressurized flames in housings as long as optical access is provided.

In Fig. 15 the mean particle diameters measured at 12 mm above the burner surface in flames with different equivalence ratios are summarized. Good agreement was found in the overlapping regions where two or even all three methods are applicable. The soot precursors (modes A+B), which also have been found with SMPS are distinquishable with PIMS for equivalence ratios equal to or below 1.9. The soot particle sizes (mode C) measured with PIMS are omitted in the diagrams because of the reasons discussed above. The LII diagnostic is not able to distinguish between different modes but the measurements are corresponding to soot because larger particles are dominating the LII signal. The soot particle size measurements obtained with LII are in good agreement with the soot sizes measured with SMPS.

In Fig. 16 the variation in particle sizes for different heights above the burner at a fixed equivalence ratio are shown. In this case the two kinds of soot precursor particles cannot be distinguished due to the excess of mode A. There are two reasons for the discrepancy of the soot particle sizes between LII and SMPS at HAB $\geq$ 13 mm. First, as discussed in 2.2, the lack of temperature data and assumption of one single temperature for all measurement conditions for the investigated flames causes an apparent decrease of particle sizes determined with LII higher in the flame. Second the SMPS probe gets clogged rather quickly when measuring at positions with high soot concentrations, which may cause an additional error.

In Fig. 17 an overview of the flame conditions where mono- or bimodal particle size distribution functions have been found is illustrated. With an

increasing equivalence ratio as well as with increasing height above the burner surface the structure of the PSDF is changing from monomodal to bimodal. The steps in Fig. 17 resemble a hyperbola and suggest the following interpretation. In this range the equivalence ratio corresponds to the concentration of soot precursors and the height above the burner is related to the reaction time. The obvious message of Fig. 17 is that the product of precursor concentration and time requires a minimum value for the formation of soot.

4 Conclusion

Three different particle sizing methods - photo-ionization mass spectrometry (PIMS), scanning mobility particle sizing (SMPS) and laser-induced incandescence (LII) - have been applied to well defined premixed laminar ethylene/air flames. We worked out the advantages and limitations of these methods and found good agreement at the flame conditions where two or even all three methods are applicable. Furthermore we generated a dataset of these ethylene/air flames for different flame conditions which will be useful for soot model validation and consequently for further understanding of the kinetics of soot formation.

References

[Axelsson 2000] Axelsson, B., Collin, R. and Bengtsson, P. E. (2000) Laser-induced incandescence for soot particle size measurements in premixed flat flames. *Applied Optics*, 39, 3683-3690.

[Bladh 2004] Bladh, H., Bengtsson, P.-E. (2004) Characteristics of laser-induced incandescence from soot in studies of a time-dependent heat- and mass-transfer model. *Applied Physics B*, 78, 241-248.

[Brackmann 2002] Brackmann, C., Bood, J., Bengtsson, P.-E., Seeger, T., Schlenk, M., Leipertz, A. (2002) Simultaneous vibrational and pure rotational CARS for temperature and multispecies concentration measurements demonstrated in sooting flames. *Applied Optics*, 41, 3.

[Braun-Unkhoff 1998] Braun-Unkhoff, M., Chrysostomou, A., Frank, P., Gutheil, E., Lueckerath, R., and Stricker, W. (1998) Experimental and numerical study on soot formation in laminar high pressure flames. *Twenty-Seventh Symposium (International) on Combustion*, 1565-1572.

[De Filippo 2007] De Filippo, A., Commodo, M., Minutolo, P., Sgro, L. A. (2007) The evolution of nanoparticle size distributions and UV-visible extinction and fluorescence in premixed ethylene air flames. *Proceedings of the European Combustion Meeting*, Paper 14-11.

[De Filippo 2007a] De Filippo, A., Sgro, L. A., and Lanzuolo, G. (2007) The evolution of nanoparticle size distributions in premixed ethylene air flames. *Proceedings of the European Combustion Meeting*, Paper 14-10.

[Dobbins 2002] Dobbins, R. A. (2002) Soot inception temperature and the carbonization rate of precursor particles. *Combustion and Flame*, 130, 204-214.

[Gonzalez Baquet 2005] Gonzalez Baquet, T., Barth, K., Grotheer, H., and Aigner, M. (2005) Mass spectrometric detection of flame generated nanoparticles (NOC) in the exhaust gas of vehicle engines. *Proceedings of the European Combustion Meeting*, Paper 61.

[Gonzalez Baquet 2007] Gonzalez Baquet, T., Grotheer, H.-H., Aigner, M. (2007) Simultaneous detection of two types of soot precursing particles using photo-ionization mass spectrometry (PIMS). *Rapid Communications in Mass Spectroscopy*, 21, 4060-4064.

[Gonzalez Baquet 2008] Gonzalez Baquet, T.; PhD (to be published), German Aerospace Center.

[Grotheer 2004] Grotheer, H. H., Pokorny, H., Barth, K. L., Thierley, M., and Aigner, M. (2004) Mass spectrometry up to 1 million mass units for simultaneous detection of primary soot and of soot precursors (nanoparticles) in flames. *Chemosphere*, 57, 1335-1342.

[Kasper 1997] Kasper, M., Siegmann, K., and Sattler, K. (1997) Evaluation of in situ sampling probe for its accuracy in determining particle size distributions from flames. *Journal of Aerosol Science and Technology*, 28, 1569-1578.

[Kock 2006] Kock, B. F., Tribalet, B., Schulz, C., and Roth, P. (2006) Two-color time-resolved LII applied to soot particle sizing in the cylinder of a Diesel engine. *Combustion and Flame*, 147, 79-92.

[Malarski 2005] Malarski, A., Beyrau, F., Leipertz, A. (2005) Interference effects of C2-radicals in nitrogen vibrational CARS thermometry using a frequency-doubled Nd:YAG laser. *Journal of Raman Spectroscopy*, 36, 102-108.

[Maricq 2004] Maricq, M. M. (2004) Size and charge of soot particles in rich premixed ethylene flames. *Combustion and Flame*, 137, 340-350.

[Maricq 2006] Maricq, M. M. (2006) A comparison of soot size and charge distributions from ethane, ethylene, acethylene, and benzene/ethylene premixed flames. *Combustion and Flame*, 144, 730-743.

[Melton 1984] Melton, L. A. (1984) Soot diagnostics based on laser heating. *Applied Optics*, 23, 2201-2208.

[Michelsen 2003] Michelsen, H. A. (2003) Understanding and predicting the temporal response of laser-induced incandescence from carbonaceous particles. *Journal of Chemical Physics*, 118, 7012-7045.

[Michelsen 2007] Michelsen, H. A., Liu, F., Kock, B. F., Bladh, H., Boiarciuc, A., Charwath, M., Dreier, T., Hadef, R., Hofmann, M., Reimann, J., Will, S., Bengtsson, P., Bockhorn, H., Foucher, F., and Geigle, K. P., Mounaim-Rousselle, C., Schulz, C., Stirn, R., Tribalet, B., Suntz, R. (2007) Modeling laser-induced incandescence of soot: a summary and comparison of LII models. *Applied Physics B*, 87, 503-521.

[Santoro 2002] Santoro, R. J., Shaddix, C. R. (2002) Laser-Induced Incandescence in applied combustion diagnostics, Ed. Kohse-Hoeinghaus and Jeffries. *Taylor and Francis. New-York.*, Chapter 9, 252 ff.

[Schulz 2006] Schulz, C., Kock, B. F., Hofmann, M., Michelsen, H., Will, S., Bougie, B., Suntz, R., and Smallwood, G. (2006) Laser-induced incandescence: recent trends and current questions. *Applied Physics B*, 83, 333-354.

[Sgro 2007] Sgro, L. A., De Fillipo, A., Lanzuolo, G., and D'Alessio, A. (2007) Observation of nanoparticles in hydrocarbon-air flames. *International Workshop on Combustion generated fine Particles. Anacapri/Italy.*

[Singh 2005] Singh, J., Patterson, R. I. A., Kraft, M., and Wang, H. (2006) Numerical simulation and sensitivity analysis of detailed soot particle size

distribution in laminar premixed ethylene flames. *Combustion and Flame*, 145, 638-642.

[Snelling 2004] Snelling, D. R., Liu, F., Smallwood, G. J., and Guelder, O. L. (2004) Determination of the soot absorption function and thermal accomodation coefficient using low fluence LII in a laminar coflow ethylene diffusion flame. *Combustion and Flame*, 136, 180-190.

[Thierley 2007] M. Thierley, H.-H. Grotheer, M. Aigner, Z. Yang, A. Abid, B. Zhao and H. Wang. (2007) On existence of nanoparticles below sooting threshold. *Proceedings of the Combustion Institute*, 31, 639-647.

[TSI] private communication

[Tsurikov 2005] Tsurikov, M. S., Geigle, K. P., Krueger, V., Schneider-Kuehnle, Y., Stricker, W., Lueckerath, R., Hadef, R., and Aigner, M. (2005) Laser-Based Investigations of soot formation in laminar premixed flames at atmospheric and elevated pressures. *Combustion Science and Technology*, 177, 1835-1862.

[Zhao 2003] Zhao, B., Yang, Z., Wang, J., Johnston, M., and Wang, H. (2003) Analysis of soot nanoparticles in a laminar premixed ethylene flame by scanning mobility particle sizer. *Aerosol Science and Technology*, 37, 611-620.

[Zhao 2003a] Zhao, B., Wang, H., and et al., (2003) Measurement and numerical simulation of soot psdf in a laminar premixed ethylene-oxygen-argon flame. *Combustion and Flame*, 133, 173-188.

[Zhao 2005] Zhao, B., Wang, H., and et al., (2005) Particle size distribution function of incipient soot in laminar premixed ethylene flames: effect of flame temperature. *Proceedings of the Combustion Institute*, 30, 1441-1448.

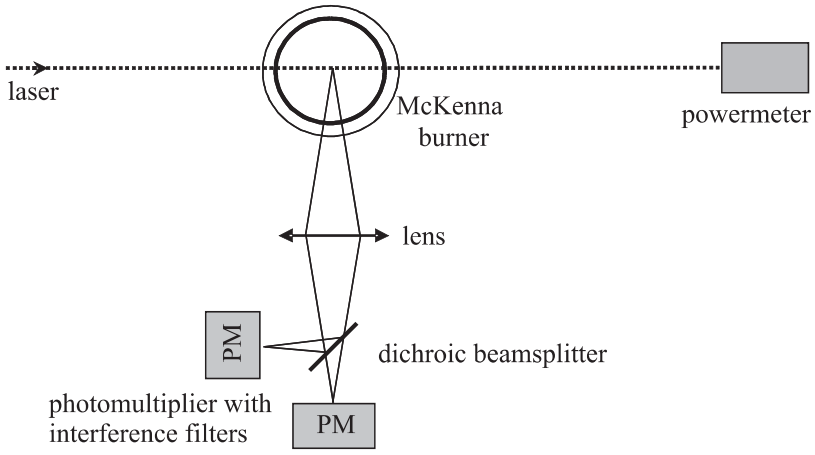

Figure 1: Experimental setup for time resolved LII measurements

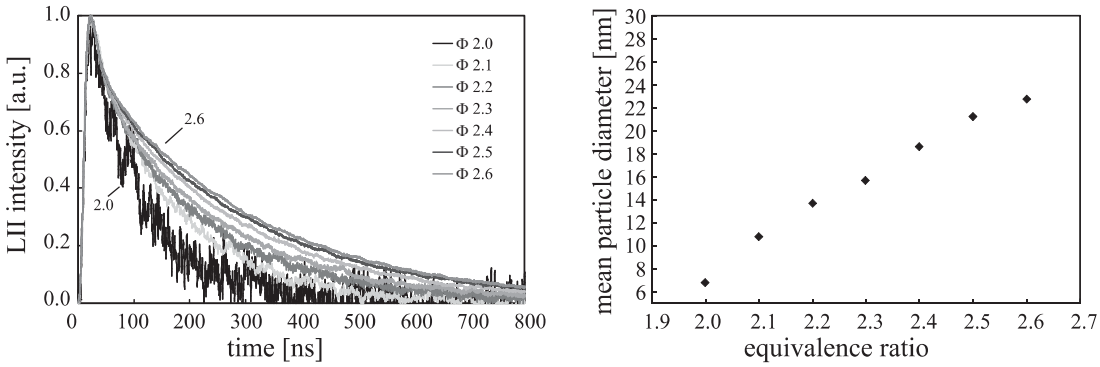

Figure 2: LII signal as a function of the equivalence ratio at 12 mm above the burner surface and the resulting particle diameters

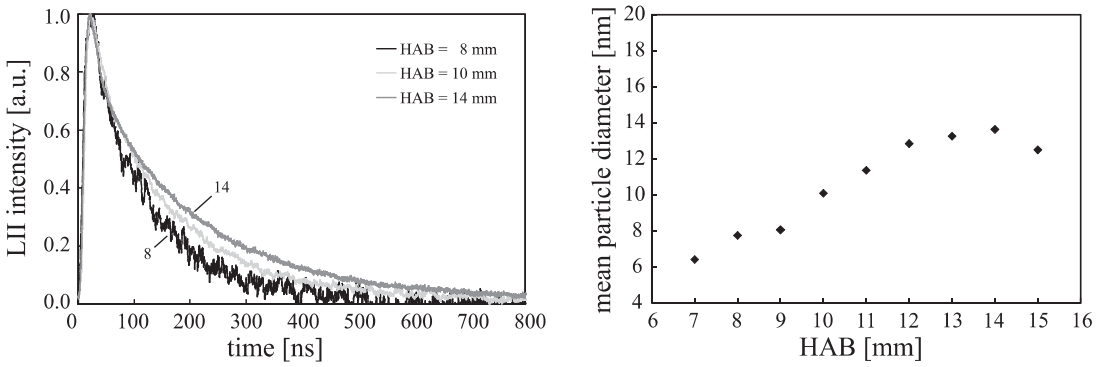

Figure 3: LII signals as a function of the height above the burner at an equivalence ratio of $\Phi = 2.1$ and the resulting particle diameters

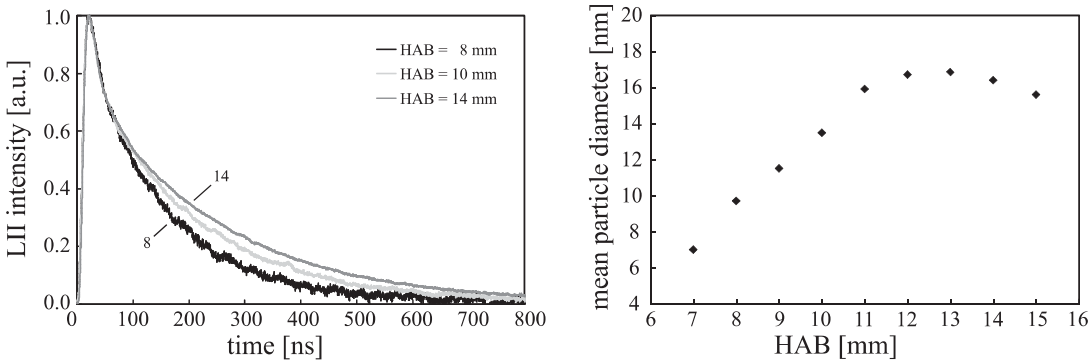

Figure 4: LII signals as a function of the height above the burner at an equivalence ratio of $\Phi = 2.3$ and the resulting particle diameters

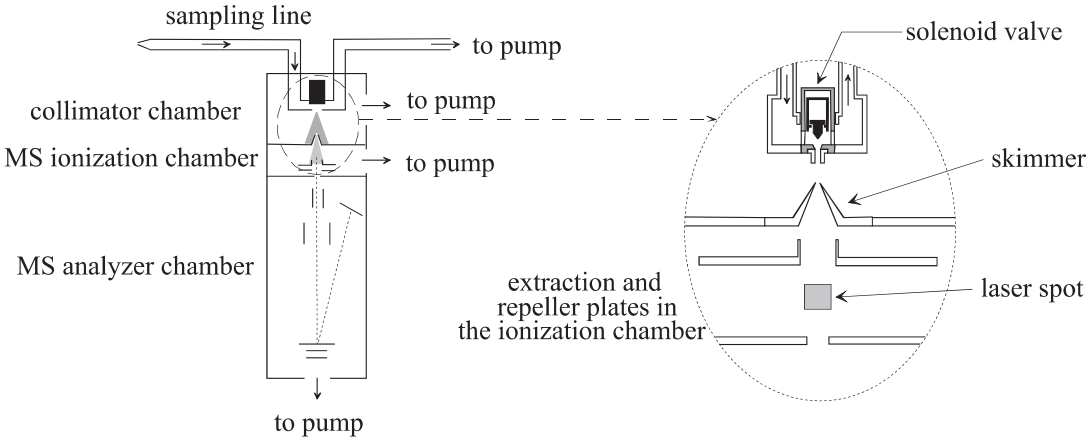

Figure 5: Schematic representation of the pulsed sampling system coupled to the time-of-flight mass spectrometer.

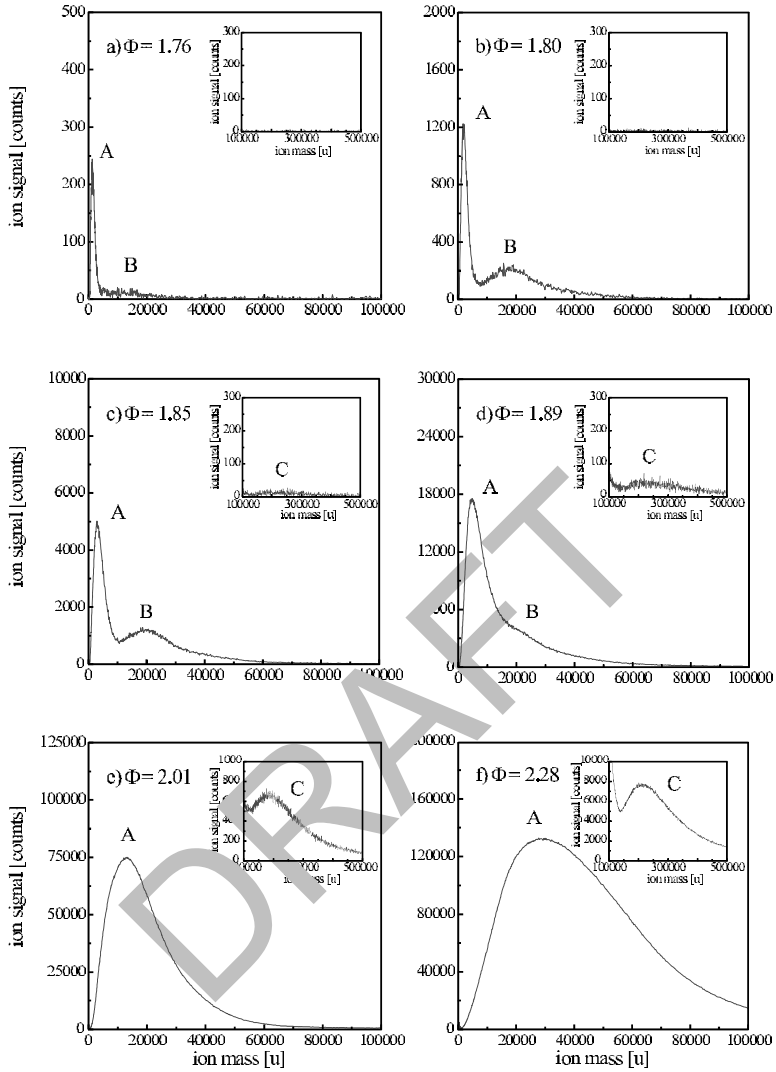

Figure 6: Average particle mass distributions measured with PIMS at $HAB = 12\ mm$ and different equivalence ratios. a) $\Phi = 1.76$. b) $\Phi = 1.80$. c) $\Phi = 1.85$. d) $\Phi = 1.89$. e) $\Phi = 2.01$. f) $\Phi = 2.28$. Note the different scales of the y axis.

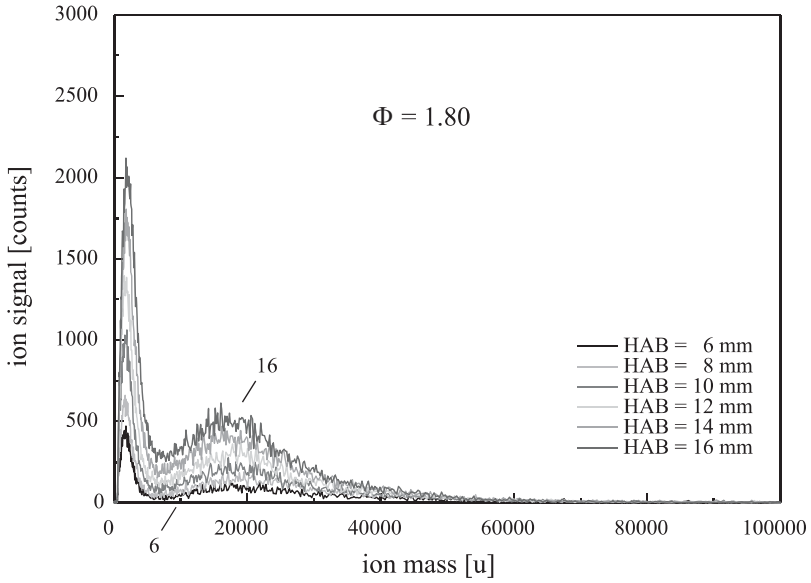

Figure 7: Particle mass distributions measured with PIMS at $\Phi = 1.80$ and different HAB.

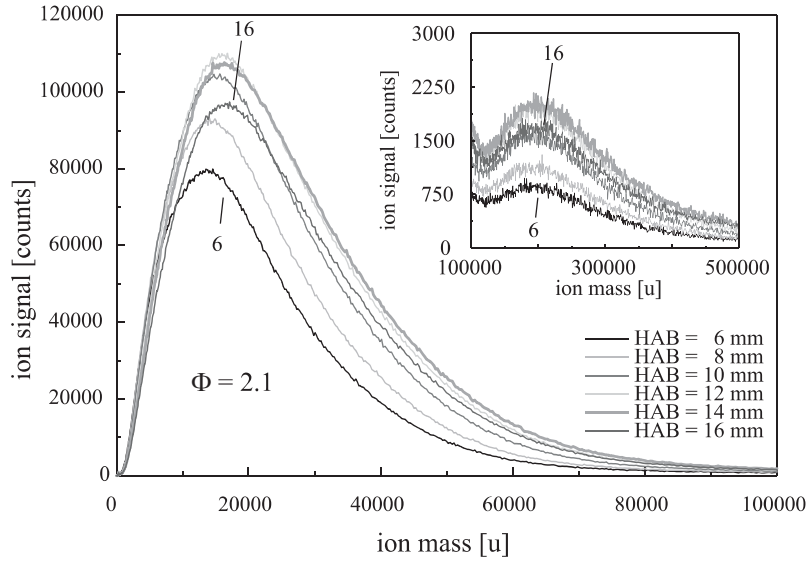

Figure 8: Particle mass distributions measured with PIMS at $\Phi = 2.10$ and different HAB.

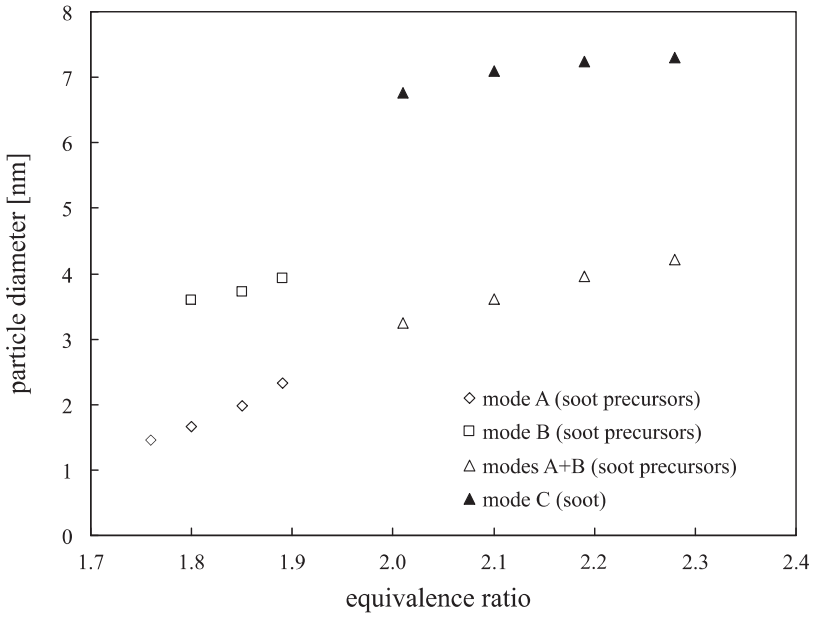

Figure 9: Mean particle diameter measured with PIMS vs. Φ at $HAB = 12\,mm$.

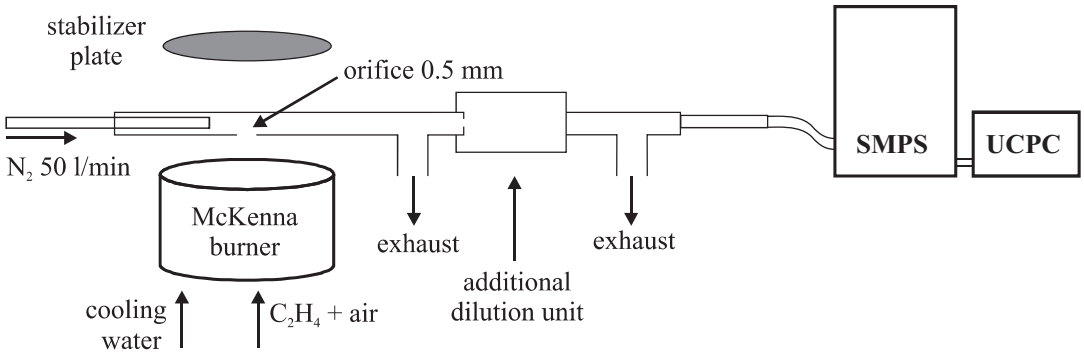

Figure 10: Schematic of the sampling system of the scanning mobility particle sizer

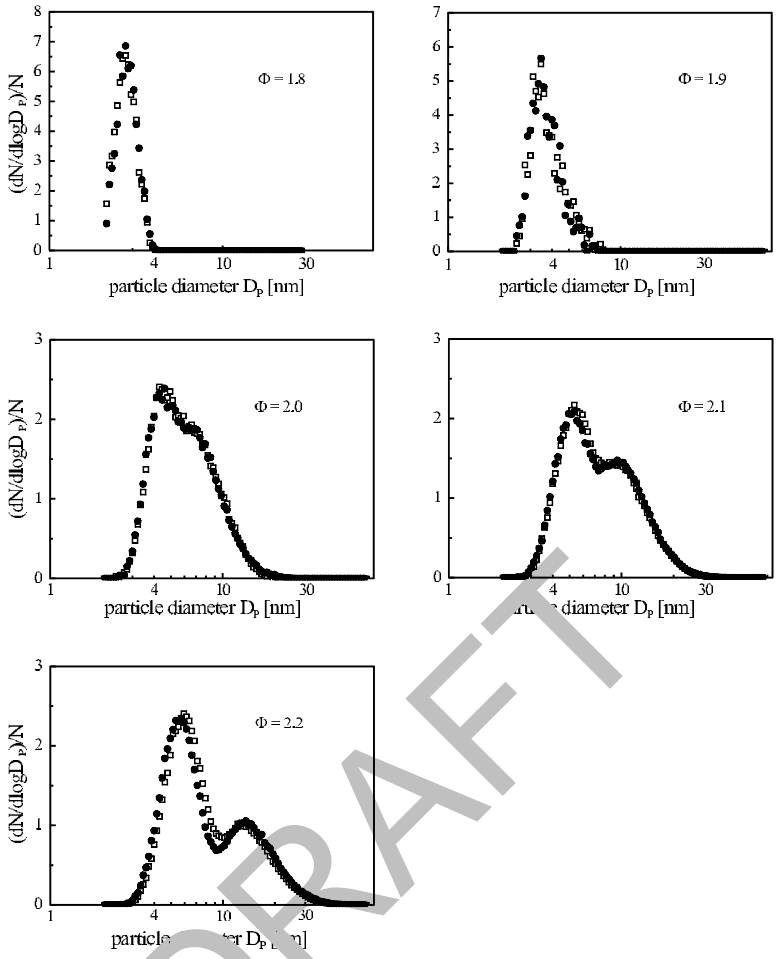

Figure 11: Normalized particle size distributions measured with SMPS at $HAB = 12\ mm$ and at different equivalence ratios (two series of measurements)

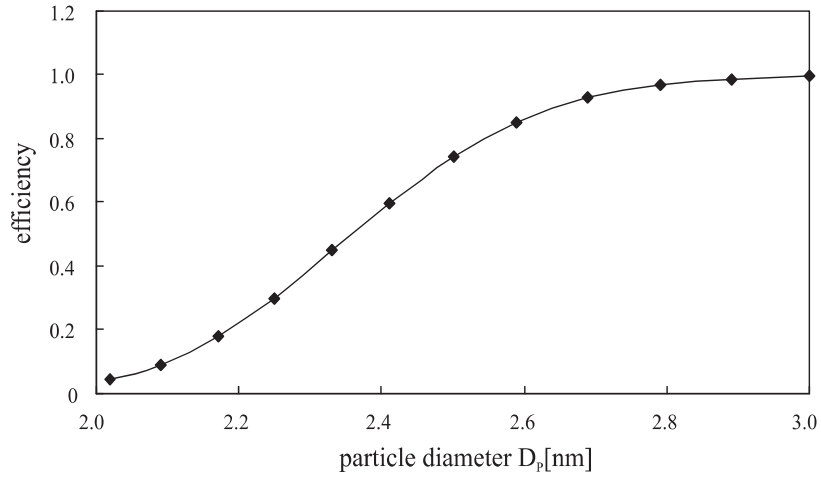

Figure 12: Counting efficiency of the TSI SMPS Model 3080 for particle sizes below 3 nm

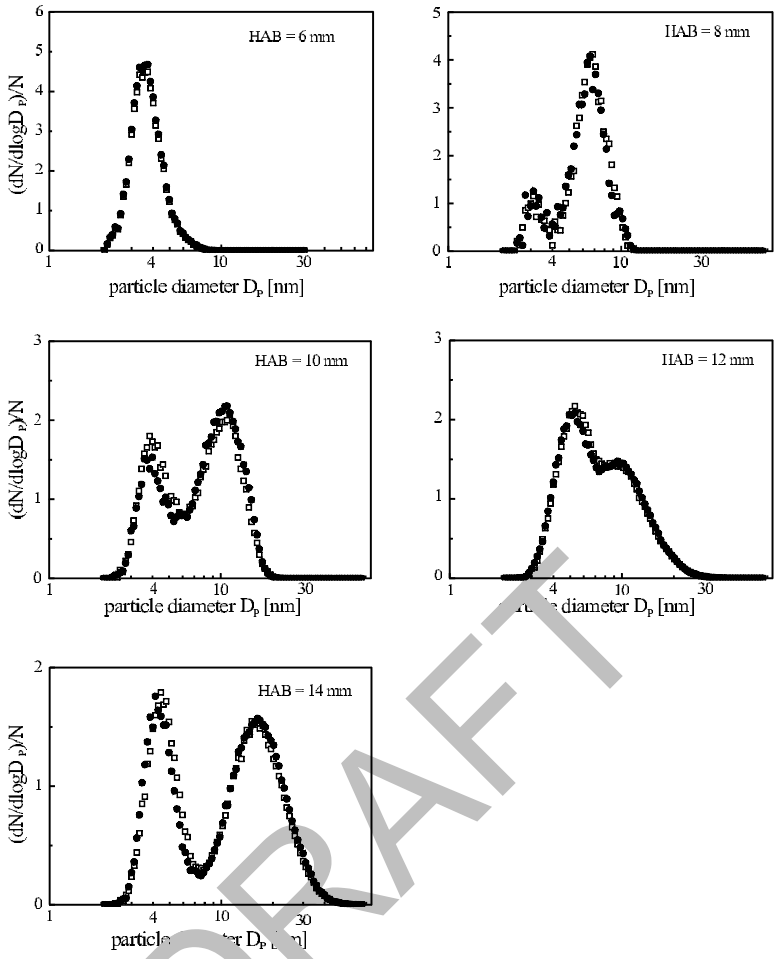

Figure 13: Normalized particle size distributions measured with SMPS at different HAB with equivalence ratio $\Phi = 2.1$ (two series of measurements)

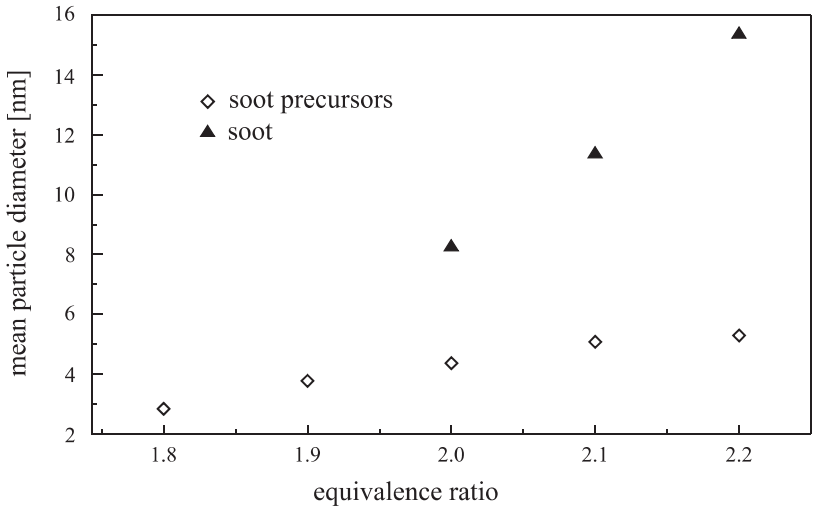

Figure 14: Mean particle diameters of the particle size distributions measured with SMPS at $HAB = 12\ mm$ and at different equivalence ratios.

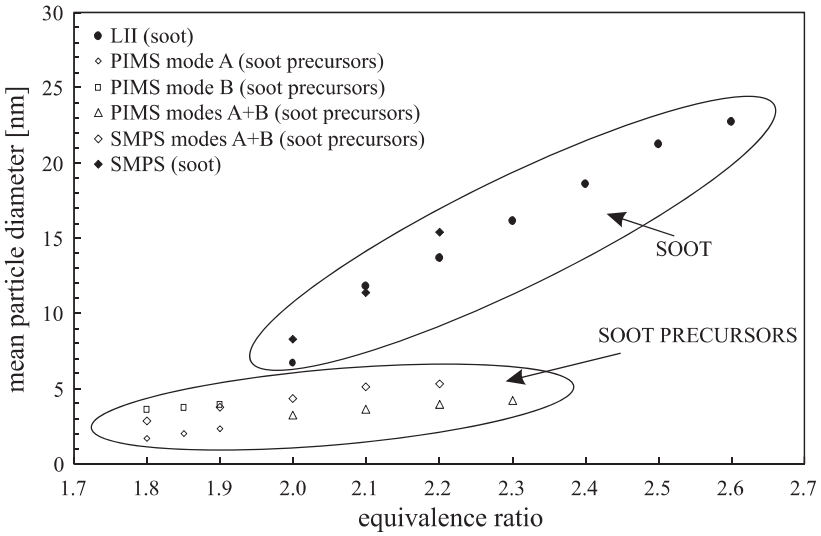

Figure 15: Comparison of the mean particle diameters for different equivalence ratios at 12 mm above the burner surface

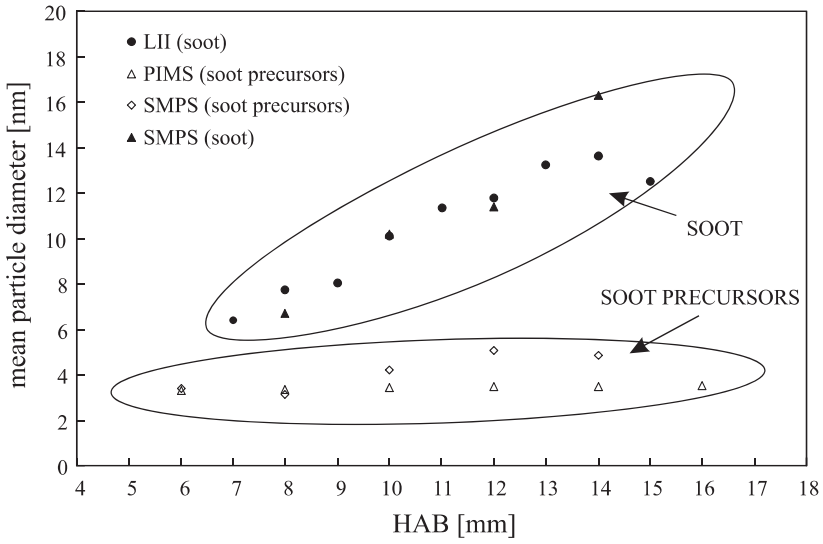

Figure 16: Comparison of the mean particle diameters for different HAB in the flame with an equivalence ratio of 2.1

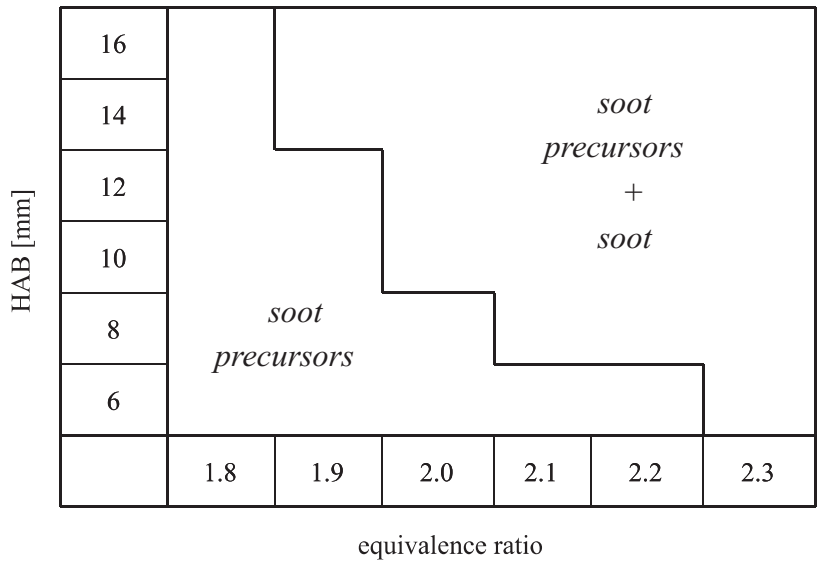

Figure 17: This diagram shows the flame conditions where we found mono- or bimodal distributions as a function of the equivalence ratio and the height above the burner surface